

Evaporation dynamics and sedimentation pattern of a sessile particle laden water droplet

G. Corkidi^{1,2} · F. Montoya^{1,2} · G. Hernández-Cruz^{2,3} · M. Vargas⁴ · J. L. Luviano-Ortíz⁵ · E. Ramos^{2,3}

Received: 24 December 2015 / Revised: 17 April 2016 / Accepted: 29 April 2016 / Published online: 25 May 2016
© Springer-Verlag Berlin Heidelberg 2016

Abstract The dynamics of the flow inside an evaporating sessile droplet of water with polystyrene micro-spheres of 1.0 μm in diameter in suspension is described. The initial volume of the droplets is in the range from 0.6 to 1.0 μl , and observations were made in the last stages before total evaporation. The flow was recorded in a sequence of images that were analyzed with a micro-PIV system to extract quantitative information. Also, using image analysis techniques we determined the dynamics of the retreating liquid film once unpinned from the original contact line. Additionally, we have explored its correlation to the formation of the sediment pattern which is organized in elongated mounds roughly deposited in azimuthal and radial orientations. It is found that the aggregation dynamics of micro-spheres in the segments of the two orientations is different. This might have a substantial influence on the final arrangement of micro-spheres in the sediments.

Keywords Sessile droplet · Evaporation · Image analysis

1 Introduction

The present study is motivated by the recently recognized possibility of using the drying process of small drops of liquid with particles in suspension deposited on solid substrates for micromanipulation. As the liquid of the sessile drop evaporates, a complicated interaction of physical effects takes place inside the drop and at the liquid–vapor–solid contact line. As a result, a multitude of deposit patterns can be formed. The specific sediment pattern contains useful information on the drying process and has been used for instance in the printing industry (Galliker et al. 2012) and to diagnose diseases (Brutin et al. 2010). In principle, the physical processes may be manipulated to control the way that the material in suspension is deposited on the substrate. The deposition and drying processes have been used to stretch (‘comb’) long molecules like DNA, (Bensimon et al. 1995), manufacture and handle nanowires (Ondarcuhu and Joachim 1998) and form nanoporous films (Wang et al. 2001). The identified applications and many potential ones have triggered a large number of studies of the main fundamental physical processes occurring inside the evaporating sessile drops.

Studies of drop evaporation date back to the classical paper by Maxwell at the end of the XIX who studied the case of an spherical drop in an infinite medium. He considered that the process was dominated by diffusion, and assumed that the vapor concentration at the wet surface of the sphere C_s is equal to its equilibrium concentration, and that the mass flux is driven by the vapor concentration difference between the surface of the drop and the concentration far away from the drop. According to Picknett and Bexton, shortly after Maxwell’s study, the evaporation of a sessile drop was considered by Sreznevsky (Picknett and Bexton 1976). The obvious difference between the two

✉ E. Ramos
erm@ier.unam.mx

¹ Laboratorio de Imágenes y Visión por Computadora, Instituto de Biotecnología, 62250 Cuernavaca, Mor., Mexico

² Universidad Nacional Autónoma de México, Mexico City, Mexico

³ Renewable Energy Institute, 62580 Temixco, Mor., Mexico

⁴ Instituto Tecnológico de Zacatepec, 62780 Zacatepec, Mor., Mexico

⁵ Department of Mechanical Engineering, Universidad de Guanajuato, Salamanca, Gto., Mexico

geometrical conditions is that in a sessile drop, the region that is in contact with the solid does not evaporate, and thus, the total mass exchange is reduced. More modern studies have dealt with the evaporation of sessile drops of pure liquids. Two general behaviors have been identified: drops whose footprint reduces as it evaporates and drops where the contact line remains fixed for most of the process. When the drop is deposited on the substrate, assuming that there are no temperature gradients and that the vapor concentration in the surroundings promotes evaporation, the rate of mass loss per unit surface area per unit time of the drop depends on the transfer rate across the liquid–vapor interface and on the diffusive relaxation of the saturated vapor layer above the drop. For times larger than R^2/D , where R is the contact-line radius and D is the diffusivity of the vapor in air, the second effect is dominant (Deegan et al. 2000).

The evaporation of drops with particles in suspension has many features in common with the evaporation of drops of pure liquids, but it has also important differences that are brought about due to dynamic interaction between the liquid and the particles. The pattern of sediments of a drying drop with particles in suspension contains a great deal of information on the substances that compose the drop and their dynamic and chemical interaction. For this reason, it has been proposed as a diagnostic mechanism in many applications, notably in medicine and in materials processing, including soft matter. Recent informative reviews on the sediment transport and patterns can be found in references (Larson 2014; Thiele 2014; Sefiane 2014).

The variety of the sediment patterns reported in the literature are very large. The simpler sediment distributions are, a single ring that forms near the initial contact line, a central mound and a uniform deposit in the whole footprint of the drop. More complex geometry sediments include multiple rings, cellular and lamellar structures, sawtooth and dendritic patterns, Serpinsky gaskets and others. Some of these structures have been described in detail in the literature. See for instance references (Deegan 2000; Bhardwaj et al. 2010).

The diversity of the sediment patterns of drying drops is the result of the hydrodynamic, electrostatic, evaporative, thermal, undulatory and other interactions between the substrates, fluids, atmospheres and materials in suspension or dilution. The interactions may occur at different time and space scales. Here, we briefly comment relevant information available in the literature focusing on monodisperse suspensions of spheres in water.

The formation of the sediment pattern is a process that starts in the early stages of evaporation and finishes shortly before total evaporation. Two examples of processes that start as soon as the drop is deposited on the substrate are: the convective flows generated by preferential evaporation

near the (pinned) contact line that drag particles toward the edge of the drop to form a circular deposit, and the formation of a central mound of particles carried by flows driven by surface tension gradients due to latent heat of evaporation (Marangoni effect). The sediment pattern is also shaped at later stages of the evaporation process when the receding liquid film pins and unpins on the substrate and leaves behind particle clusters of various forms. A large variety of sediment patterns that form in this final stages have been reported. The geometry of the sediment depends on the initial concentration, diameter of the particles, electrostatic and van der Waals forces, etc. See for instance (Deegan 2000; Bhardwaj et al. 2010).

Attempts to model these mechanisms have been developed, and many important features have been properly captured. The dynamics of sediment formation that take place in the early stages have been modeled by integrating Navier–Stokes equations in a volume that reduces as the drop evaporates. The motion of the spheres is incorporated in the model with Brownian dynamics (Hu and Larson 2006). Also, the sediment formation has been modeled using a Lagrangian framework for the continuous phase and an advection diffusion equation to track the particle concentration (Bhardwaj et al. 2009). Widjaja and Harris (2008) predicted particle concentrations using a finite element numerical model solving a continuum advection–diffusion equation coupled with a deposition model for the particle–substrate interaction based on the electrical double layer (Spielman and Friedlander 1974). A theoretical model aimed at predicting the formation of deposit structures in the final stages of the evaporation when the liquid film recedes has been presented by Frastia et al. (2011). The model is based on a lubrication equation for hydrodynamics coupled with a mass balance equation for the concentration of particles and predicts the regular and irregular line patterns of sediments due to self-organized pinning–unpinning cycles corresponding to a stick–slip motion of the contact line.

In the present study, we observe the dynamics of the liquid evaporation in sessile drops of water with microspheres in suspension. We focus on the last stages of the evaporation when the drop is formed by a thin liquid film still attached to the original contact line and in the last stage when the film detaches from the contact line and the liquid undergoes total evaporation.

2 Experimental techniques

The optical technique used to obtain the images was a phase contrast illumination setup under an inverted Olympus IX71 microscope with a UplanFL N 4x objective and a high-speed camera Optronis 5000 running at a rate of 60

fps and with a resolution of 512×512 pixels. The size of the field of view was $2500 \times 2500 \mu\text{m}$, and the depth of field is $<3 \mu\text{m}$. The light source was a 660 nm wavelength Thorlabs, USA, M660L2 LED.

In all observations, the targets were distilled water droplets with volumes in the range of 0.6–1.0 μl with fluorescent micro-spheres in suspension (Thermoscientific fluorescent micro-spheres). Droplets were deposited on a round VWR micro cover borosilicate glass substrate. No special treatment to the surface of the substrate was made. The temperature was kept constant at 14 °C with a Bipolar Temperature Controller CL-100 (Warner Instruments, USA) coupled to a Peltier device SC-20 series platform (Warner Instruments, USA) and a RE415 Cooling Thermostat (Lauda-Königshofen, Germany). The environmental relative humidity was 30–48 %. We used the image analysis software Image-Pro version 7.0 to trace semiautomatically the contour of the contact line while the droplet was evaporating. This was achieved by using the autotracing edge detection procedure selecting at least two sample points in such border region, so the algorithm could follow the remaining contour of the breaking contact line automatically. The coordinates of the rupture contours were saved in text format to integrate them with the PIV results. To estimate the number of micro-spheres per unit volume, we used a Neubauer chamber and a grain counting image analysis procedure that measures the total intensity of light emitted by the micro-spheres in a known liquid volume, subtracting the background light and dividing by the average light emitted by a single particle. The droplets with volumes of 1 μl have initial footprints of approximately 2 mm in diameter ($2R$) and the suspensions used have 3.20×10^5 – 5.67×10^6 micro-spheres per μl . For the PIV analysis, we used interrogation areas of 16×16 pixels ($78 \times 78 \mu\text{m}$) and 25 % overlap. The process was observed by recording the evolution of the droplet profile as the liquid evaporates.

The capillary length¹ $\lambda_c \sim 2.7$ mm, and the bond number $B_o = \rho g (2R)^2 / \gamma$ is 0.54 which indicates that surface tension is the dominant effect that determines the initial shape of the droplet. As it is well known, in this case, the shape of the droplet is closely approximated by a spherical cap. In the characterization of the orientation of the traces formed by the droplet after evaporation, and for the determination of the local delays defined in Sect. 5 at both sides of azimuthal and radial traces, home-made routines were used.

¹ $\lambda_c = \sqrt{\gamma / \rho g}$. The surface tension is $\gamma = 72 \times 10^{-3}$ Nw/m, the gravity acceleration and density are, respectively, $g = 9.8$ m/s² and $\rho = 997$ kg/m³.

3 Evaporation dynamics

In the first part of the evaporation process, the motion inside the droplet is a toroidal convective cell with radial symmetry which is generated to compensate the larger evaporation near the contact line (Hu and Larson 2005; Kang et al. 2004). If the droplet contains micro-spheres in suspension, the radial velocity (u_r) near the substrate drags the micro-spheres and piles them up at the rim of the droplet forming a circular deposit known as the *coffee ring* as explained by Deegan et al. (1997). Near the end of the evaporation process, the droplet is almost flat and the velocity field inside the droplet is mostly radial even though the preferential evaporation near the contact line is small. When the liquid film is sufficiently thin and rips off from the sediment ring, the internal flow is driven by a complicated interaction between evaporation and the surface tension which pulls the liquid to minimize the area. The receding liquid moves toward the center of the droplet leaving behind a thin trailing film that evaporates fast but which is determinant for the formation of the sediment pattern as explained in Sect. 5.

3.1 Evaporation times and evaporation rates

The total time of evaporation of a sessile droplet depends on the volume, the temperature and the ambient relative humidity. In the range of volumes explored and for the prevailing ambient parameters, the processes last typically several minutes. We confirmed the observation made by other authors that the initial contact angle for both, drops with and without micro-spheres, in suspension is approximately 43° and reduces linearly with time as the evaporation proceeds (Hu and Larson 2002). However, for pure water droplets, the linear reduction of the contact angle stops at approximately 12° when surface tension pulls the remaining liquid toward the central region of the droplet and forms a droplet with smaller, and often noncircular footprint. In contrast, the liquid in the droplets with micro-spheres in suspension remains attached to the original contact line. As it is well known, this behavior is due to the fact that the micro-spheres tend to accumulate at the rim of the droplet and form a porous medium where the surface tension exerts a much larger linear force that fixes the liquid.

Theories for estimating the evaporation time of a sessile droplet have been presented by Picknett and Bexon (1976), Hu and Larson (2002) and Marin et al. (2011b). The developments include the case of fixed footprint area which is the case of most interest here. Hu and Larson give the following expression for the evaporation rate \dot{m} obtained by curve fits to a model based on an accurate numerical solution of the diffusion equation in a semi-infinite domain where the droplet is immersed:

Table 1 Total evaporation times and evaporation rates for droplets with micro-spheres in suspension

	$C \times 10^{-6}$ part/ μl	t_e (s)	$\dot{m}_e \times 10^6$ (gr/s)	t_t (s)	$\dot{m}_t \times 10^6$ (gr/s)	Δt (s)	$\Delta \dot{m}$ (gr/s)
I	2.50	750	1.61	666	1.80	11.2	-12.1
II	2.50	612	1.96	680	1.76	-11.1	10.3
III	2.50	612	2.00	680	1.80	-11.2	10.4
IV	5.70	456	2.12	475	2.03	-4.2	4.4
V	5.70	534	1.96	538	1.94	-0.7	1.1
VI	5.70	540	2.05	566	1.94	-4.9	5.0
VII	5.70	600	2.03	583	2.08	2.8	-2.5

Particle concentration: C . Experimental evaporation time: t_e , and experimental evaporation rate: $\dot{m}_e = -dm/dt|_e$. Theoretical time from Eq. 1: t_t , and theoretical evaporation rate ($\dot{m}_t = -dm/dt|_t$). Percent difference in evaporation times: $\Delta t = (t_e - t_t)/t_e * 100$ and percent difference in evaporation ratios: $\Delta \dot{m} = (\dot{m}_e - \dot{m}_t)/\dot{m}_e * 100$

$$-\dot{m} = \pi R D (1 - H) c_V (0.27\theta^2 + 1.30), \quad (1)$$

where R is the radius of the droplet footprint, D is the water vapor diffusion coefficient in air, H is the relative humidity, c_V is the water vapor saturation coefficient and θ is the initial contact angle. The rate of evaporation depends on the ambient temperature through the equilibrium water vapor concentration. It was observed that the evaporation times and rates of droplets with micro-spheres in suspension have smaller dispersion and are better predicted with the theories than those of pure water. For concentration of 2.50×10^6 micro-spheres/ μl , the difference with theoretical predictions of Hu and Larson (2002) is smaller than 10 % and for concentration of 5.70×10^6 micro-spheres per μl the difference is smaller than 5 % which is comparable to the accuracy of the experiment (Table 1). As explained before, the contact line for the droplets with micro-spheres in suspension remains fixed, while for pure water it retracts at a relative early stage of the process. Also, we have observed that the contact line of droplets of pure water is continuously moving during the evaporation process and the collecting angle is much larger ($\sim 12^\circ$) than that for droplets with micro-spheres.

3.2 Velocity field inside the droplet near the substrate

We now describe the velocity field inside the droplet captured with the 2D micro-PIV. In the observations of this subsection, the drop has reduced to a thin liquid film attached to the ring of sediment accumulated at the contact line. It is interesting to note that the processes described in this section constitute the last 1.5 % of total evaporation time. The motion in the radial direction is dominant, although complex local motion has also been observed. In order to illustrate the process, we show the velocity field in Fig. 1. This velocity field was obtained 20.0 s before total evaporation, which will be labeled $t = -20.0$ s, taking $t = 0$ s at total evaporation. In the central region ($r < 0.3 R$),

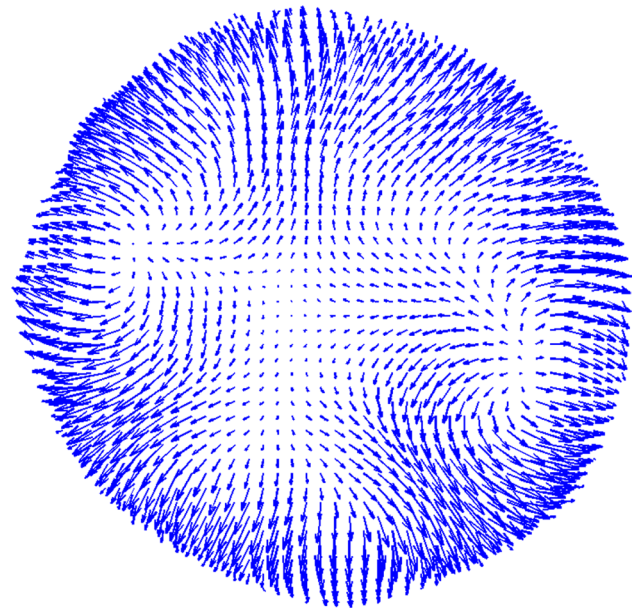


Fig. 1 Velocity field at $t = -20.0$ s (20.0 s before total evaporation). The image was taken 8 μm above the substrate

the radial velocity is small, approximately one third of the maximum observed velocity, and for $r > 0.9 R$ and up to the contact line, the flow is radial with small azimuthal and vertical components, but for the intermediate region, $0.3 R < r < 0.9 R$, three mass source-like spots where evaporation at the surface of the droplet is hindered can be identified. The interaction of the velocity field in the vicinity of these regions with the overall field generates local spots of nonzero azimuthal velocities. A more quantitative picture of the velocity distribution and the scales of the motion is given in Fig. 2. In the upper panel (Fig. 2a), the instantaneous radial velocity is shown as a function of the azimuthal coordinate for $r = 0.8 R$ and several times. As it is discussed with greater detail below, at $t = -11.5$ s, the liquid film rips from the peripheral sediment. At $t = -20.0$

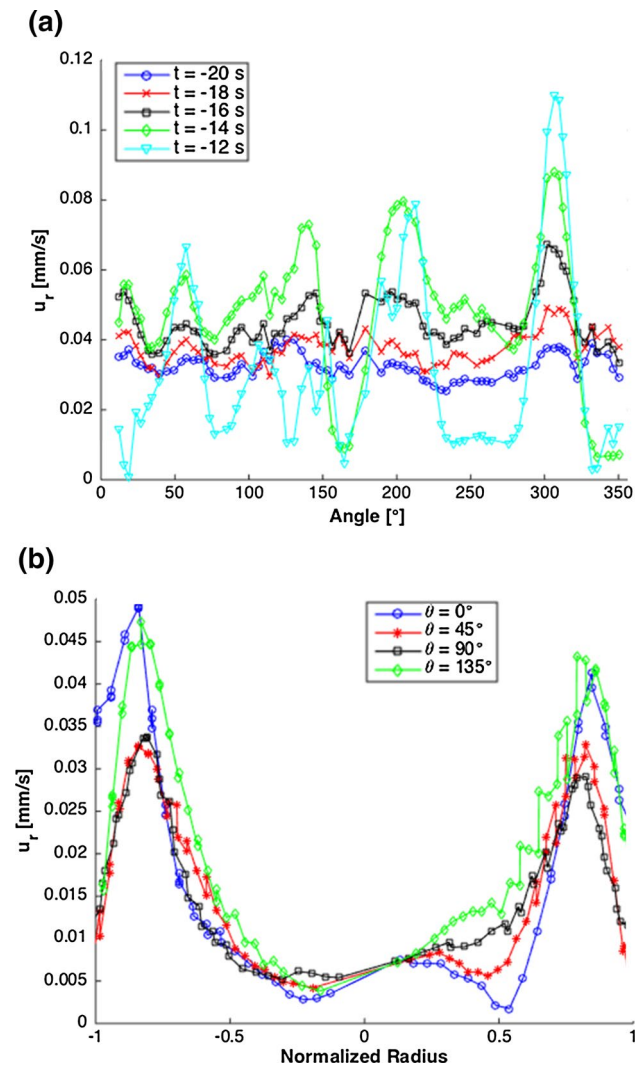


Fig. 2 Radial velocity profiles inside the drop. **a** Radial velocity as a function of the polar angle θ for several times and $r = 0.8 R$, **b** radial velocity as a function of radius for several angular positions at time -15.3 s

s, the velocity field is nearly a constant radial velocity of approximately 0.035 mm/s; note that at this time, the liquid is practically a film with maximum height of $8 \mu\text{m}$. Shortly after, at $t = -12.0$ s, the local flows manifest themselves as maxima at 50° , 140° , 200° and 300° with maximum velocities of up to 0.090 mm/s indicating a substantial acceleration and a clear departure from azimuthal symmetry. This phenomenon indicates that in some orientations the retracting film is favoured and in some others the film sticks to the substrate. At later times, roles may change generating jerks in the contractions which may be determinant for the geometry of the sediment (see Sect. 5).

Figure 2b shows the radial velocity as a function of the radius for different angular positions and before the liquid film detaches from the circular sediment ($t = -15.3$ s).

Although not perfectly symmetric, the velocity distribution displays two maxima of average 0.038 mm/s at $r \sim \pm 0.8 R$ and a central plateau with $u_r = 0.005$ mm/s.

4 Observations of the dynamics inside the droplet

In order to illustrate the details observed in the last stages of evaporation, we show a representative example in Fig. 3.

The upper row of Fig. 3 shows the inverse optical microscopy images of the last stages of evaporation for a droplet with a concentration of 5.70×10^6 micro-spheres per μl . In the lower row, the corresponding velocity field occurring inside the droplet is shown. In these figures, the thickness of the liquid film is $< 8 \mu\text{m}$ and the flow is mostly two-dimensional. In the first column of Fig. 3, the liquid fills the whole circular area and the internal flow is mostly radial with an approximate azimuthal symmetry and drags micro-spheres toward the contact line. The characteristic velocity of the liquid as a function of time is estimated by recording the radial component on rings of constant radii and averaging over their length. We have considered rings of radii $0.8 R$ and $0.3 R$ and show the results in Fig. 4. At early times (~ -20.0 s) and for $0.8 R$, the average radial velocity is a monotonously increasing function of time, up to a point where it reaches a maximum of approximately 4.50×10^{-2} mm/s. Then, the radial velocity diminishes due to the receding motion of the film that moves with an opposite velocity relative to the motion of the micro-spheres. The trace for $r = 0.3 R$ presents similar qualitative features but interesting quantitative differences. The radial velocity for $r = 0.3 R$ at early times (~ -20.0 s) is about an order of magnitude smaller than that observed at $0.8 R$, but the maximum velocity reached at $r = 0.3 R$ is nearly twice as large as the maximum observed at $0.8 R$. This clearly demonstrates that the outward velocity liquid accelerates even though the liquid contact line is moving inwards with a velocity comparable with that of the micro-spheres suspended in the fluid. The traces show a maximum that is displaced toward larger times for smaller radii. The gradual acceleration observed at the two radial positions is consistent with the hyperbolic growth proposed by Marin et al. (2011b) and can be described by the expression $C/(t_f - t)$ where t_f is the time for the maximum value of the velocity. In the figure, we include best fit hyperbolas. The velocity readings from rings with large radii stop at an earlier time than that with smaller radius indicating that the dry zone grows from the contact line inwards. The trace for $r = 0.3 R$ displays a double maximum which results from a non-symmetric process showing that the averaging over fixed rings is not representative of the whole process. Once the liquid film separates from the circular sediment at the original contact line, the shape of the liquid zone is strongly

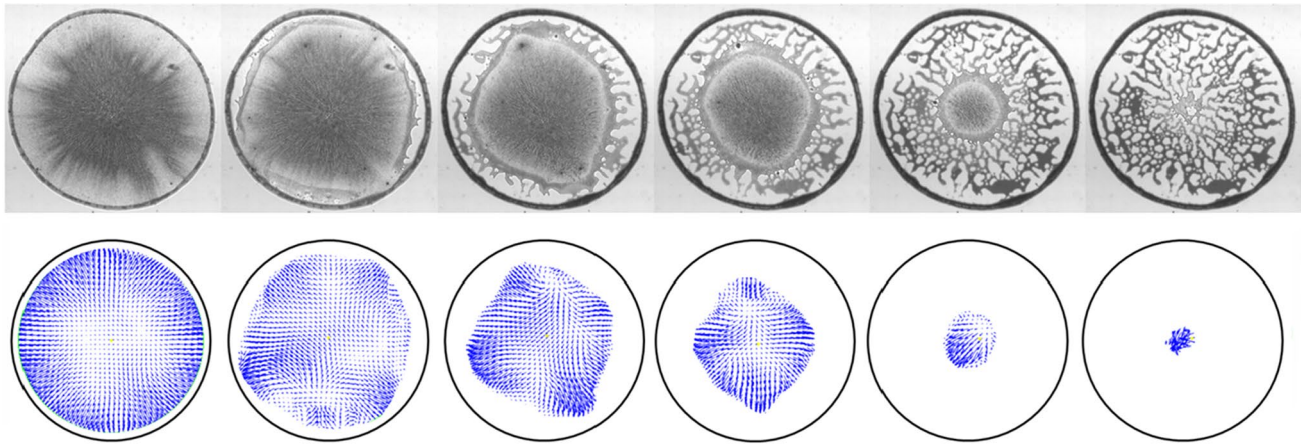


Fig. 3 Last stages of evaporation for a $1.0 \mu\text{l}$ droplet, 5.70×10^6 micro-spheres per μl in suspension and 2 mm footprint. *Upper row*, inverse optical microscope images. *Lower row* micro-PIV veloc-

ity fields. Defining the $t = 0 \text{ s}$ at total evaporation, the images and velocity fields in each column were taken from *left to right* at -20.5 , -11.5 , -7.3 , -4.8 , -1.5 and 0.0 s

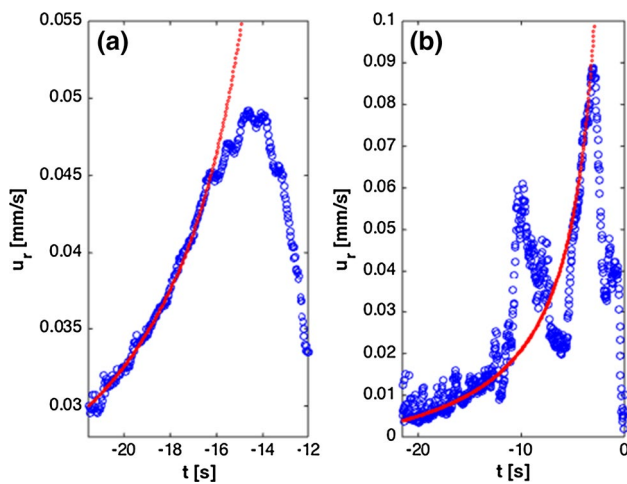


Fig. 4 Average radial velocity as a function of time; the radial velocity was averaged over *circles* that are concentric with the original *contact line*. **a** $r = 0.8 R$, **b** $0.3 R$. The *broken lines* are the hyperbolas that best fit the initial part of the data; the origin of time ($t = 0$) coincides with total evaporation

asymmetric and critically depends on local effects. These include partial attachment of the liquid film to the peripheral circular sediment, zones with nonuniform accumulation or depletion of micro-spheres, and others.

After enough material has evaporated, the liquid film breaks away from the ring formed by sphere sediments and recedes toward the center of the droplet, leaving behind a circular sediment. The places where the separation starts depend on the local details of the ring at the original contact line and are difficult to capture with the optical technique used in the present investigation. Once the liquid film detaches from the ring of sediment, it moves inward forming approximate smaller and smaller circles as the

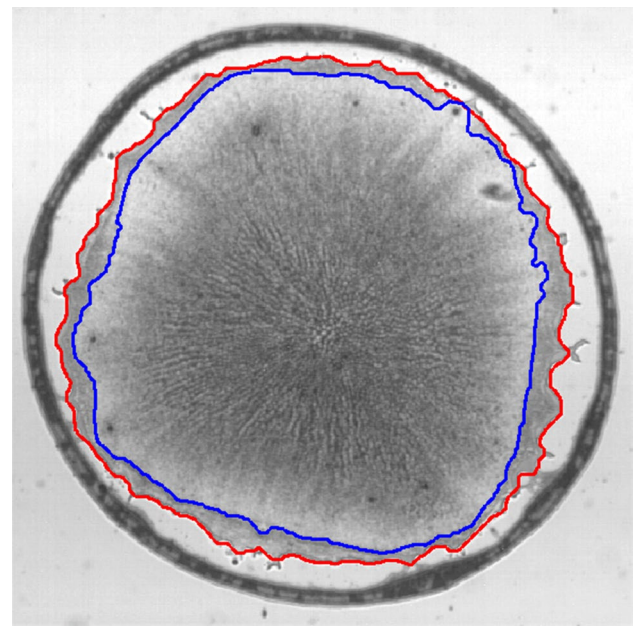


Fig. 5 As the droplet evaporates, the liquid bulk (area encircled by *blue line*) retreats leaving behind a film of liquid (area between *red and blue lines*). The image was taken at $t = -8.4 \text{ s}$

liquid is depleted by evaporation. A structure formed by two clearly identifiable zones is developed; the inner part is a relatively thick film that contains small micro-spheres in suspension and a much thinner film that completely wets the surface of the substrate. This thin film is akin to the precursor film that forms when a wetting droplet spreads out on a substrate (DeGennes et al. 2004), and we label this as the *trailing film*. Figure 5 illustrates the structure of the receding droplet when it has just entirely detached from the coffee ring. The position where the droplet presents a

large gradient in thickness can be accurately found since it presents a sharp change in gray intensity. The receding line of the trailing presents small amplitude perturbations. It has been observed that the dynamics of the trailing film and the distribution of the suspended micro-spheres have a large influence on the pattern of the sediment. The process of evaporation and the motion of the receding line of the trailing film leave behind the micro-spheres that aggregate in groups and form the sediment. It is observed that the sediment is formed by relatively thick, circular arcs of sediment that suggest the formation of secondary coffee rings; see third to sixth columns of Fig. 3.

5 Analysis of the sediment patterns

In this section, we look into the geometrical properties of the sediment after total evaporation and its possible correlation with the drying dynamics. Although the pattern of residues is the result of the overall process that includes the uneven particle concentration on early stages of the evaporation, the last stage is crucial to determine the geometry of the sediment distribution that remains after total evaporation. Here, we will describe a correlation found for the geometry of the sediment segments in terms of local velocity features.

Once the liquid unpins from the circular contact line, the average motion of the film is in the radial direction as the film contracts from the initial contact line toward the center of the droplet. The nonuniform retraction of the liquid film forms elongated mounds of sediment which will be called *filaments*. We find that the sediment filaments are oriented in the radial and azimuthal directions (segments of circles); in order to quantify this observation, we make a classification of the orientation of the sediments. To this end, first we extract the position of the medial line of the elongated sediments using a medial axis transform (Gonzalez and Woods 2008) to obtain the skeleton of the sediment pattern (one pixel width representation of the sediment pattern, see white lines in Fig. 6a). For every point of the skeleton, it is possible to define its position vector R with respect to the center of the droplet and a vector T tangent to the skeleton on that specific point. Figure 6b shows the schematic construction of R and T . The dashed line represents the skeleton of a trace, and the vectors V_{il} and V_{ir} represent the position of the i th neighbors nearest to R , the left and right ones, respectively. Taking n neighbors from each side of R (from the 2nd to the 5th), T_i can be defined as $T_i = V_{ir} - V_{il}$; then, by averaging these vectors, T can be defined as $T = 0.25 \sum_{i=2}^5 T_i$ representing a reasonably good approximation to the local tangent of the skeleton. Only the directions of R and T are needed, their magnitudes being irrelevant for the purpose of this work.

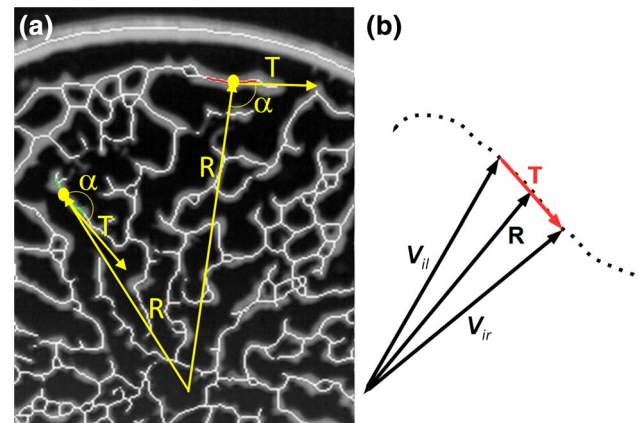


Fig. 6 Illustration of the geometrical classification of the traces as radial (green) or azimuthal (red). The variable R denotes position vectors with the origin of coordinates at the center of the droplet. The distribution of sediments is shown in gray and the medial line (or skeleton) are the white lines

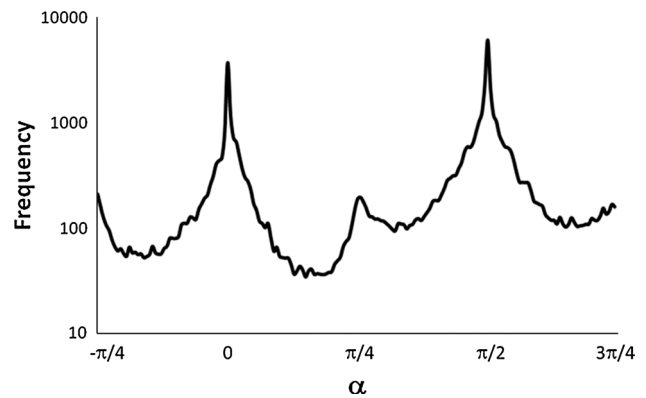


Fig. 7 Semi-logarithmic plot of the distribution of the orientation of traces

The histogram of the orientation angles of traces is shown in Fig. 7. As can be appreciated, the bimodal distribution indicates that indeed, the orientation of most of the segments is close to 0 or $\pi/2$. The radial and azimuthal orientations are defined when $-\pi/4 < \alpha \leq \pi/4$ and $\pi/4 < \alpha \leq 3\pi/4$, respectively. The result of the application of the whole procedure is shown in Fig. 8 where the original distribution of sediments and the orientation classification in radial or azimuthal are shown with the two color code. The dynamics of the formation of sediment traces was inferred by calculating the local velocity of the trailing film and by finding the position of the film for subsequent times; this was achieved by dividing the difference of distances between local positions of the trailing film at consecutive time intervals. To this end, the position of the retreating trailing film during the final stages of the evaporation process was captured in a sequence of images

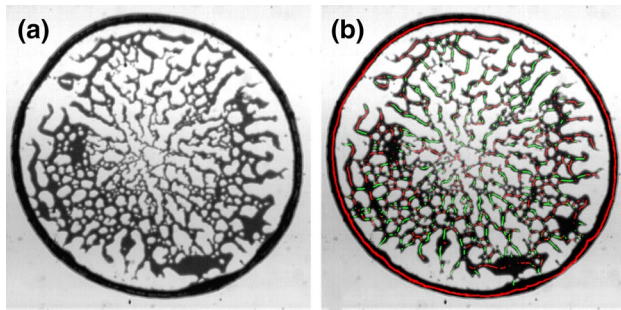


Fig. 8 Orientation of the sediment traces. **a** Original distribution of sediments, **b** orientation of sediment traces: *green* and *red* correspond to radial and azimuthal segments, respectively

at 60 fps for roughly 23 s. A subsampled set (by a factor of 16) of 88 snapshots was obtained and the edge of the film extracted by image difference processing. We then make a composition of the images of the drying droplet and record the position of the edge of the trailing film as shown in Fig. 9a. Each image was obtained 267 ms after the previous one. The actual pattern of the sediment is the result of the complex interaction of the evaporation of the liquid film and the accumulation of micro-spheres near the substrate that fix the film to specific spots. As noted by Deegan (2000), this effect occurs as the liquid film evaporates because the micro-spheres are trapped into the wedge of fluid next to the contact line, preventing it from retracting. Nadkarni and Garoff (1992) observed that even a single particle can fix the film but when a number of micro-spheres accumulate in the same region, the cohesion forces due to surface tension increase due to the increase in the effective area. The detachment of the film starts in dry spots where liquid has evaporated or retracted. In this way, the motion of the contact line is a sequence of pinned and unpinned states. This process leaves a trail of deposits that can be classified in radial and azimuthal elongated segments of clusters of micro-spheres. It is observed that the retracting film runs parallel near the outer side of azimuthal sediments, while in the inner side the motion of the liquid film is approximately perpendicular to the deposit. This is indicated by arrows 1 and 2 in Fig. 9b. For the regions between filiform sediments oriented in the radial direction, it is observed that the trailing film moves between two filaments of micro-spheres forming a concave contact line since the film that touches the sediments lags behind the contact line far away from the filaments. The local retracting speed can be inferred from the distance between the images of the edges of the liquid film obtained at different times. An example is indicated by arrows 2 and 3 in Fig. 9b. The result of the full process is shown in Fig. 9c. At this point, a very interesting feature was observed: the orientation of most of the shape-elongated

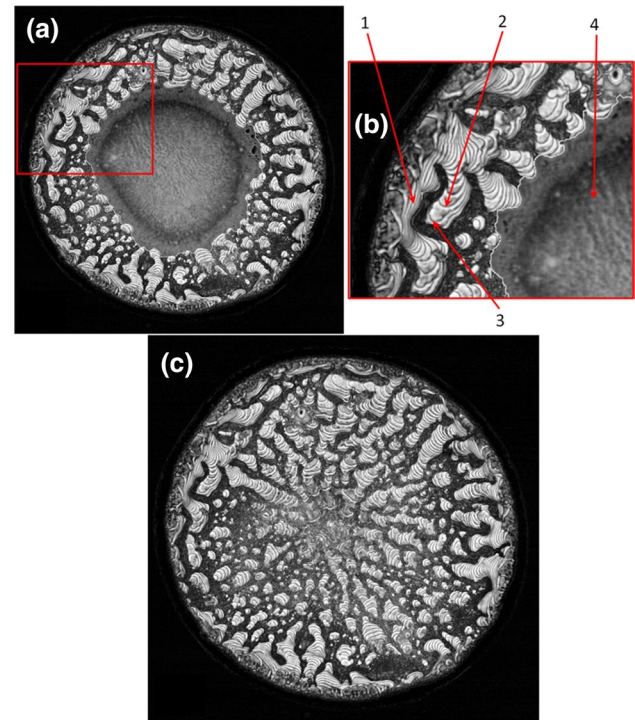


Fig. 9 Composite image of 88 snapshots taken at time intervals of 267 ms, showing the subsequent positions of the trailing film. The *light gray* areas with strips correspond to zones where the film is receding while the *darker areas* are sediment agglomerations. **a** Image showing the ongoing evaporation process. **b** Detail from the previous figure. *Arrows 1* and *2* indicate flow directions at the sides of an azimuthal sediment. Observe that the motion indicated by *arrow 1* is parallel to the deposit. In contrast, *arrow 2* indicates that the motion is perpendicular to the deposit. *Arrow 3* indicates the relative large distance from the strip pointed by *arrow 2*, corresponding to a high-speed evaporating. In the region indicated by *arrow 4* is the remanent of the liquid droplet still to be evaporated, **c** image covering the whole evaporating history

sediments, classified as radial or azimuthal, is correlated with the delay existing between the instant when the flow dries at the sides of that specific sediment. In order to quantify this observation, we take the following steps. First, we extract the position of the medial line (skeleton) of the elongated sediments. Then, the line normal to each point in the medial line is drawn and its extreme points, defined as the points farthest from the center falling inside the sediment, are found. These geometrical definitions are shown in Fig. 10. The receding motion of the liquid film is different for azimuthal and radial segments: In the azimuthal segments, for example points (a_1, a_2) in Fig. 10a, the time elapsed between the dewetting of one of the extremes of the normal line is 3.1 s longer than that of the other extreme. In contrast, for a radial segment (points (b_1, b_2)), the dewetting occurs almost simultaneously, i.e., $\tau \sim 0$. These observations are illustrated in Fig. 10b where the time series show the instantaneous variance of the

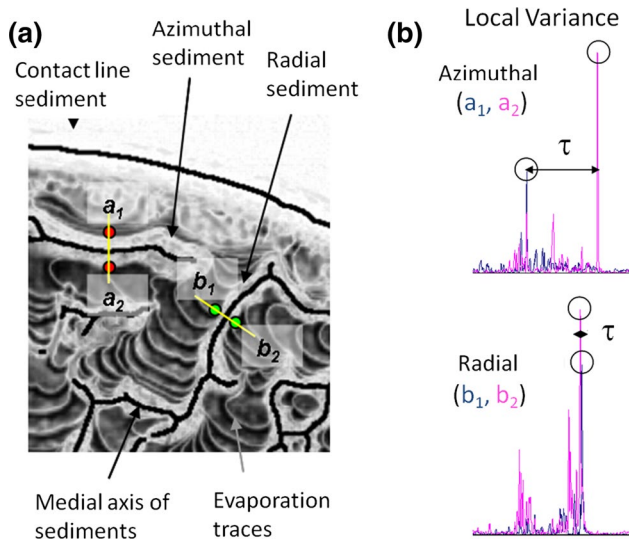


Fig. 10 Orientation of most of the shape-elongated sediments is correlated with the delay existing between the instant when the flow dries at both sides of the border of that specific sediment (classified as radial or azimuthal). **a** Points a_1, a_2 for a azimuthal trace, b_1, b_2 for a radial one, **b** the spiky signals are the time series of local intensity variance for the marked points. The global maximums (encircled in the figure) represent the drying instant for a particular position; $\tau > 0$ for an azimuthal trace (top) and $\tau \sim 0$ for a radial one (bottom)

intensity profile over points a_i, b_i (pink or dark for $i = 1, 2$, respectively), defined by the equation:

$$\sigma(t, X) = \frac{1}{\Delta t} \sum_{i=t}^{t+\Delta t} (I(i) - \bar{I})^2, \tag{2}$$

where t is time, X is the position of observation over points a_i, b_i , Δt is the window size that gives the instantaneous meaning to the variance, and I and \bar{I} are the intensity and the average intensity of the original time series recorded, respectively. For this work, Δt is equal to 10, which represents three orders of magnitude smaller than the time series; for this reason, the instantaneous assumption of the variance is justified. The global maximum of the instantaneous variance represents the dewetting instant of a particular position within the image. The time delay (τ) of the dewetting instant between both sides of the traces is the experimental observable which correlates with the orientations.

The process of the agglomeration of the sediment should have a major influence on the structural properties of the micro-spheres in the sediment. As explained in reference (Marin et al. 2011a), the distribution of the micro-spheres in the outermost circular sediment is initially ordered (crystalline) and then disordered due to the velocity at which the micro-spheres are accreted on the sediment. We expect that the particle deposition dynamics on one side of the azimuthal filaments is similar to that occurring in the

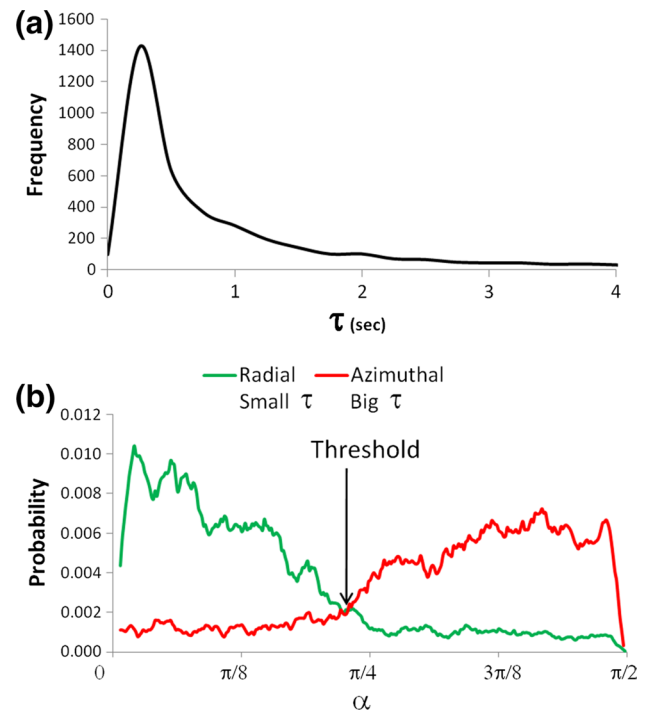


Fig. 11 **a** Distribution of the orientation of traces. **b** Small and large τ probability distribution and threshold

circular sediment described by Marin et al. (2011a), as can be inferred from the fact that the motion of the contact line and also of the micro-spheres dragged by the trailing film is radial, almost parallel to the filament; see the azimuthal filament highlighted in Fig. 9b (arrows 1 and 3). In contrast, for radial filaments, the deposition of micro-spheres is made almost simultaneously on the two sides and as can be guessed from the shape of the liquid film, the micro-spheres move radially and are then deflected to be deposited to build the sediment; see the radial filament highlighted in Fig. 10a, points (b_1, b_2) . The distribution of the time delays detected is shown in Fig. 11a where it can be seen that a large amount of cases have very small τ but also that the distribution presents a long tail reaching up more than $\tau = 4$ s.

In order to cluster the dynamic behavior of the dewetting process in two groups, we split the database in two sets, one with large τ and the other with small τ containing half the total number of data points each. Then, we plot the histograms of the orientation angles that correspond to each set of data points to obtain Fig. 11b. As can be appreciated, the histogram for small angles ($\alpha \sim 0.07$ rad [4°]) indicating a strong correlation to radial filaments. Correspondingly, the large distribution are correlated with large angles ($\alpha \sim 1.40$ rad [80°]) corresponding to azimuthal orientations. An alternative, perhaps more visual method to display the same result is given

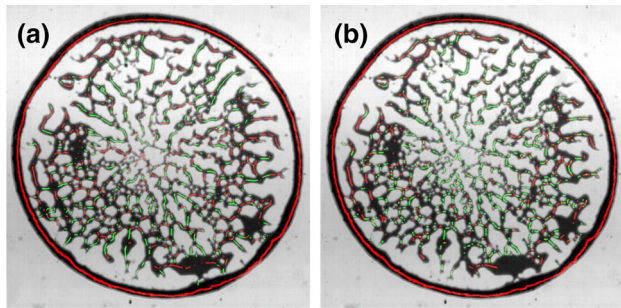


Fig. 12 Median lines of the sediment pattern classified as radial (green) or azimuthal (red). **a** Orientation of the original sediments (see Fig. 6), **b** orientation of sediments according to their corresponding τ showing evident correlation

in Fig. 12 where the orientation of the filaments obtained with the geometrical method described previously in Fig. 6 is compared with the orientation of the filaments obtained with the dynamic method described in Fig. 8. In this plot, the data for radial (azimuthal) distribution beyond the threshold $\tau > \tau_T$ ($\tau < \tau_T$) have been omitted.

6 Conclusions

We described the dynamics of the last part of the evaporation of water drops laden with polystyrene micro-spheres of 1 μm . Similar to the case of pure water drops, the total evaporation time is of the order of several minutes, with micro-spheres rapidly accumulating at the contact line, pinning down the liquid. It is found that simple theories which consider that the contact line is fixed, accurately predict the evaporation times and mass loss. The velocity fields obtained with μPIV at the end of the evaporation when the liquid is a thin film reveal a dominant radial motion that contributes to the formation of the peripheral ring of sediments. In the last seconds of the evaporation, the thin film of liquid rips from the ring of sediment and a process akin to the dewetting with a two-film structure occurs. It is found that the dynamics of the velocity of the receding outer film is related to the geometry of the sediment. Specifically, we found that the formation of azimuthal and radial filamentary mounds of sediment is different. The accumulation of micro-spheres on the two sides of the radial segments occurs simultaneously, while micro-spheres aggregate first at the outer side of the azimuthal mounds rather than at the inner side. This effect has a major role in the determination of the structure of the deposit which is strongly dependent on the dynamic details of particle drag. Of course, this does not preclude the influence of other effects like the initial particle density and distribution on the final pattern of the

sediment. We remark that the conclusions of the correlation between the dynamics of dewetting and the pattern of the sediment are more clear and easy to analyze in cases where the process displays approximate radial symmetry, but it is also true for cases where the last stages of evaporation are off the center of the main sediment ring.

References

- Bensimon D, Simon AJ, Croquette V, Bensimon A (1995) Stretching dna with a receding meniscus: experiments and models. *Phys Rev Lett* 74:4754–4757
- Bhardwaj R, Fang X, Attinger P (2009) Pattern formation during the evaporation of a colloidal nanoliter drop: a numerical and experimental study. *N J Phys* 11:075020
- Bhardwaj R, Fang X, Somasundaran P, Attinger P (2010) Self-assembly of colloidal particles from evaporating droplets: role of dlvo interactions and proposition of a phase diagram. *Langmuir* 26:7833–7842
- Brutin D, Sobac B, Loquet B, Sampol J (2010) Pattern formation in drying drops of blood. *J Fluid Mech* 667:85–95
- Deegan RD (2000) Pattern formation in drying drops. *Phys Rev E* 61:475–485
- Deegan RD, Bakajin O, Dupont TF, Huber G, Nagel SR, Witten TA (1997) Capillary flow as the cause of ring stains from dried liquid drops. *Nat Lond* 389:827–829
- Deegan RD, Bakajin O, Dupont TF, Huber G, Nagel SR, Witten TA (2000) Contact line deposits in an evaporating drop. *Phys Rev E* 62:756–765
- DeGennes PG, Brochard-Wyart F, Quéré D (2004) Capillary and wetting phenomena: drops, bubbles, pearls, waves. Springer, New York
- Frastia L, Archer AJ, Thiele U (2011) Dynamical model for the formation of patterned deposits at receding contact lines. *Phys Rev Lett* 106:077801
- Galliker P, Schneider J, Eghlidi H, Kress S, Sandoghdar V, Poulikakos D (2012) Direct printing of nanostructures by electrostatic auto-focussing of ink nanodroplets. *Nat Commun* 3:2
- Gonzalez RC, Woods RE (2008) Digital image processing, 3rd edn. Prentice Hall, New Jersey
- Hu H, Larson RG (2002) Evaporation of a sessile droplet on a substrate. *J Phys Chem B* 106:1334–1344
- Hu H, Larson RG (2005) Analysis of the microfluid flow in an evaporating sessile droplet. *Langmuir* 21:3963–3971
- Hu H, Larson RG (2006) Marangoni effect reverses coffee-ring depositions. *J Phys Chem B* 110:7090–7094
- Kang KH, Lee SJ, Lee CM, Kang IS (2004) Quantitative visualization of flow inside an evaporating droplet using the ray tracing method. *Meas Sci Technol* 15:1104–11012
- Larson RG (2014) Transport and deposition patterns in drying sessile droplets. *AIChEJ* 60:1538–1571
- Marin AG, Gelderblom H, Lohse D, Snoeijer JH (2011a) Order-to-disorder transition in ring-shaped colloidal stains. *Phys Rev Lett* 107:085508
- Marin AG, Gelderblom H, Lohse D, Snoeijer JH (2011b) Order-to-disorder transition in ring-shaped colloidal stains. supplementary material. *Phys Rev Lett* 107:085508
- Nadkarni GD, Garoff S (1992) An investigation of microscopic aspects of contact angle hysteresis: pinning of the contact line on a single defect. *Europhys Lett* 20:523–528
- Ondarcuhu T, Joachim C (1998) Drawing a single nanofibre over hundreds of microns. *Europhys Lett* 42:215–220

- Picknett RG, Bexon R (1976) The evaporation of sessile or pendant drops in still air. *J Colloid Interface* 61:336–350
- Sefiane K (2014) Patterns from drying drops. *Adv Colloid Interface Sci* 206:372–381
- Spielman LA, Friedlander SK (1974) Role of the electrical double layer in particle deposition by convective diffusion. *J Colloid Interface Sci* 46:22–31
- Thiele U (2014) Patterned deposition at moving contact lines. *Adv Colloid Interface Sci* 206:399–413
- Wang H, Wang Z, Huang L, Mitra A, Yan Y (2001) Surface patterned porous films by convection assisted dynamic self-assembly of zeolite nanoparticles. *Langmuir* 17:2572–2574
- Widjaja E, Harris MT (2008) Particle deposition study during sessile drop evaporation. *AIChE J* 54:2250–2260